Surface imaging of metallic material fractures using optical coherence tomography

Gheorghe Hutiu,[1] Virgil-Florin Duma,[1,2,*] Dorin Demian,[1]
Adrian Bradu,[3] and Adrian Gh. Podoleanu[3]

[1]3OM Optomechatronics Group, "Aurel Vlaicu" University of Arad, 77 Revolutiei Ave., Arad 310130, Romania

[2]Polytechnics University of Timisoara, 1 Mihai Viteazu Ave., Timisoara 300222, Romania

[3]Applied Optics Group, School of Physical Sciences, University of Kent, Canterbury, CT2 7NH, UK

*Corresponding author: duma.virgil@osamember.org

Received 17 June 2014; accepted 30 July 2014;
posted 5 August 2014 (Doc. ID 214127); published 4 September 2014

We demonstrate the capability of optical coherence tomography (OCT) to perform topography of metallic surfaces after being subjected to ductile or brittle fracturing. Two steel samples, OL 37 and OL 52, and an antifriction Sn–Sb–Cu alloy were analyzed. Using an in-house-built swept source OCT system, height profiles were generated for the surfaces of the two samples. Based on such profiles, it can be concluded that the first two samples were subjected to ductile fracture, while the third one was subjected to brittle fracture. The OCT potential for assessing the surface state of materials after fracture was evaluated by comparing OCT images with images generated using an established method for such investigations, scanning electron microscopy (SEM). Analysis of cause of fracture is essential in response to damage of machinery parts during various accidents. Currently the analysis is performed using SEM, on samples removed from the metallic parts, while OCT would allow *in situ* imaging using mobile units. To the best of our knowledge, this is the first time that the OCT capability to replace SEM has been demonstrated. SEM is a more costly and time-consuming method to use in the investigation of surfaces of microstructures of metallic materials.

OCIS codes: (110.0110) Imaging systems; (120.0120) Instrumentation, measurement, and metrology; (110.4500) Optical coherence tomography; (160.3900) Metals; (170.4500) Optical coherence tomography; (180.5810) Scanning microscopy.

http://dx.doi.org/10.1364/AO.53.005912

1. Introduction

Optical coherence tomography (OCT) is a recognized imaging technique based on low-coherence interferometry [1]. Initially developed for biomedical investigations like ophthalmology [2], skin, teeth, and endoscopy, its area of application has expanded toward other fields, such as materials studies, profilometry, and art applications.

In material studies OCT has been used mostly for the nondestructive testing of semiconductors [3], glass [4], composite materials, and plastic [5–7]. OCT and other techniques, such as white light interferometry, have also been used for metallic materials, for example, to determine their roughness [8]. The issue of penetration depth that is acute in imaging tissue is of no concern in this case, as such studies refer only to the profile of a reflective metallic surface.

A direction of research that, to the best of our knowledge, has not yet been approached is the investigation of the type of fracture (ductile, brittle, or fatigue). The process of a ductile fracture generates less serious problems than that of a brittle fracture, because ductile fractures do not occur instantly (as the brittle ones do); an elongation takes place

1559-128X/14/265912-05$15.00/0

before the actual fracture. This is why it is essential to identify the type of fracture, if ductile or brittle.

This analysis is important for a range of applications, including (i) to determine the causes that have generated different kinds of incidents, for example, the damage of machinery parts (e.g., in aviation, maritime, road, or rail accidents), pipe ruptures, or structural failures of metallic bridges and buildings; (ii) to optimize the design of various machinery; (iii) to obtain new data regarding the structure of solid bodies (especially of new types of alloys); (iv) to improve the manufacturing technologies of different metallic materials. Images of the surface structures of metallic materials are obtained nowadays using a variety of methods and equipment such as magnifying lenses, ordinary optical microscopes, as well as optical microscopes functioning at high temperatures, transmission or scanning electron microscopes (SEMs) [9], and atomic force microscopes.

In the present paper we shall analyze the structure of metallic materials (their fracture surfaces) previously subjected to tests for ductile [10,11] or brittle fractures [12–14]. The aim is to demonstrate the capability of OCT to replace an established method of analysis, SEM, used in such studies. The advantages and drawbacks of each method will also be discussed.

2. Methods and Materials

The surface microstructures were analyzed using two different pieces of equipment, a 10 μm resolution swept source (SS)-OCT system and a 4 nm resolution SEM.

A schematic diagram of the SS-OCT imaging system, similar to that reported in [15,16], is shown in Fig. 1. As the optical source, an SS (Axsun Technologies, Billerica, Massachusetts), with a central wavelength of 1060 nm, a sweeping range of 106 nm (quoted at 10 dB), and a 100 kHz line rate is used. The interferometer configuration uses two single-mode directional couplers, DC1 and DC2. DC1 has a ratio of 20/80, and DC2 is a balanced splitter, 50/50. DC2 feeds a balance detection receiver (Thorlabs, Newton, NJ, model PDB460C). 20% of the SS power is launched toward the object arm via lens L1 (focal length 15 mm), which collimates the beam toward a pair of scanners XYSH (Cambridge Technology, Bedford, Massachusetts, model 6115), followed by an interface optics made from a scan lens, L2 (50 mm focal length) [17]. The power to the sample S is 2.2 mW.

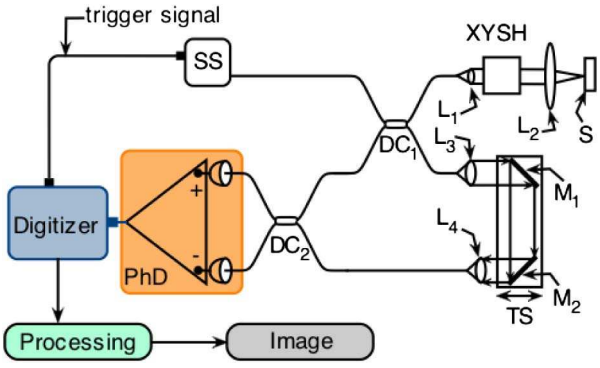

Fig. 1. Schematic diagram of the SS-OCT system. SS, swept source; DC1, 20/80 single-mode directional coupler; DC2, 50/50 single-mode directional coupler; XYSH, two-dimensional lateral scanning head; L1 to L4, achromatic lenses; S, sample; PhD, photodetector; M1 and M2, flat mirrors; TS, translation stage.

At the other output of DC1, 80% of the SS power is directed toward the reference arm equipped with flat mirrors, M1 and M2, placed on a translation stage, TS, to adjust the optical path difference (OPD) in the interferometer. Collimating lenses L3 and L4 are similar to L1. The signal from the balanced receiver is sent to one of the two inputs of a dual input digitizer (Alazartech, Quebec, Canada, model ATS9350, 500 MB/s). A trigger signal from the SS synchronizes the acquisition. The acquired channeled spectra CS (OPD) were manipulated via a program implemented in Labview 2013, 64 bit, deployed on a PC equipped with an Intel Xeon processing unit, model E5646 (clock speed 2.4 GHz, six cores).

For the SEM analysis a high vacuum FEI Quanta 250 SEM and a secondary Everhard–Thomley electron detector were used. The samples have not been metal coated. The working parameters (WD, working distance; Pa, pressure) are given below each image (Figs. 2–4), and they may vary depending on the image selected.

The samples were inserted in the microscope and examined at various magnitudes. They were mounted on a copper or aluminum conductive holder stub using carbon wafers with adhesive on both sides. The mounting of the samples was done using the lens of a binocular microscope in order to expose the investigated area directly to the electron beam scanning the sample. The sample alignment on the stub is important in this stage in order to reduce the tilting inside the microscope.

Two types of materials have been chosen: the first type (i.e., steel) is typically subjected to ductile fractures, and the second one (for which a Sn–Sb–Cu antifriction alloy has been considered) is typically subjected to brittle fractures.

The characteristics of these metallic materials for which the microstructures were analyzed after being subjected to fracture tests are:

(a) OL 37 steel (STAS 500/2-80) has the following chemical composition: C 0.18%, Mn 0.85%, S 0.04%, P 0.05%, and Fe for the rest. This steel is mainly used for the manufacturing of welded metallic parts and protection wire meshes. Its microstructure is made of ferrite and pearlite grains.

(b) OL 52 steel (STAS 500-80) has the following chemical composition: C 0.22%, Mn 1.6%, P 0.045%, S 0.045%, and Fe for the rest. This steel is mainly used for the manufacturing of welded parts, car frames, high-capacity tanks, and cranes. Its microstructure is also made of ferrite and pearlite grains.

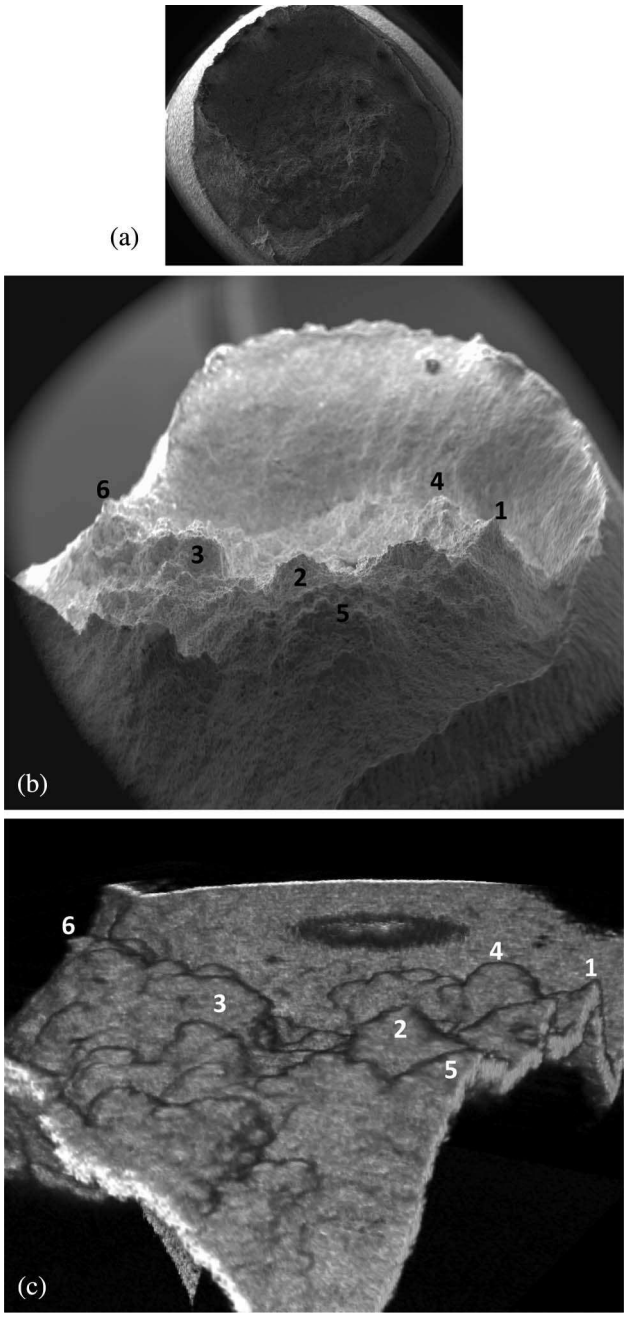

Fig. 2. Imaging the fracture of OL 37 steel: (a) frontal SEM overview of the entire sample; (b) SEM image; (c) OCT image of the same area.

(c) The Sn–Sb–Cu antifriction alloy has the following chemical composition: Sb 12%, Cu 4%, Cd 1%, and the rest Sn. It is used for the manufacturing of internal combustion engine bearings. Its microstructure consists of a soft core of a Sn solid solution containing small amounts of dissolved Cu and Sb, as well as a hard phase of SnSb and Cu_3Sn.

All the samples were subjected to tensile tests until they broke. After that, 5 mm high parts containing the cup fracture were examined using both OCT and SEM—the latter mainly for the validation of the OCT images. All the images obtained by means of the OCT and SEM comprised the same area (3.5 mm × 3.5 mm). In order to capture the same zone with both methods, a sign has been marked on the lateral margin of the sample, and SEM and OCT images were taken for the fracture zone in the vicinity of that sign. No image processing procedures were performed. However, as we shall see in the following, a good match was obtained in all the cases between the topographies of the metallic surfaces obtained with the two types of images, despite the difference in resolution between the two methods.

3. Results and Discussion

Figure 2 shows the image of a surface microstructure broken in a ductile manner belonging to the OL 37 sample. Figure 2(a) shows the image of the analyzed sample. The sample fracture has produced a cup-type shape specific for the ductile fracture. Figure 2(b) shows the SEM image of the microstructure. Figure 2(c) shows the OCT microstructure image of the same surface. Six grains were numbered on each of these two images in order to allow for the comparison of the images acquired using OCT and SEM. By comparing OCT images with images produced by the established SEM method, the utility of the OCT method for the study of microstructures of metallic surfaces can be established.

It can be seen on both images that the grains broke in a transgranular manner. This is characteristic of the ductile/shearing fracture, which is produced inside crystal grains in sliding planes with maximum atom density. Indeed, all the grains in Figs. 2(b) and 2(c) are broken, including those noted (i.e., grains 2–6): they all miss their peaks. Furthermore, the ductile fracture crack propagates along the maximum tangential stress of the load applied, i.e., under a 45° angle from the tensile stress applied. This is best seen on grain 2 [Fig. 2(c)], where the crack is both in the direction of the tensile stress and in the frontal direction of the view.

Figure 3 shows the microstructure image of an OL 52 steel sample. Figure 3(a) shows, similar to Fig. 2(a), the image of the entire analyzed sample analyzed using the SEM, with the cup-type shape specific to a ductile fracture. Figure 3(b) shows the image of the microstructure obtained by SEM analysis. Figure 3(c) shows the same microstructure obtained using OCT. Six grains were numbered on each of these two images for the comparison between the OCT and the SEM images. The same grains can be noticed, and they are all broken in a transgranular manner.

Figure 4 shows the image of the microstructure of the Sn–Sb–Cu antifriction alloy considered. Figure 4(a) shows an overview of the analyzed sample obtained via the SEM. It can be seen that the sample broke without elongation, resulting in a brittle fracture.

Figure 4(b) shows the SEM image of the same microstructure. The 3.5 mm × 3.5 mm area analyzed further on using OCT has been outlined on this

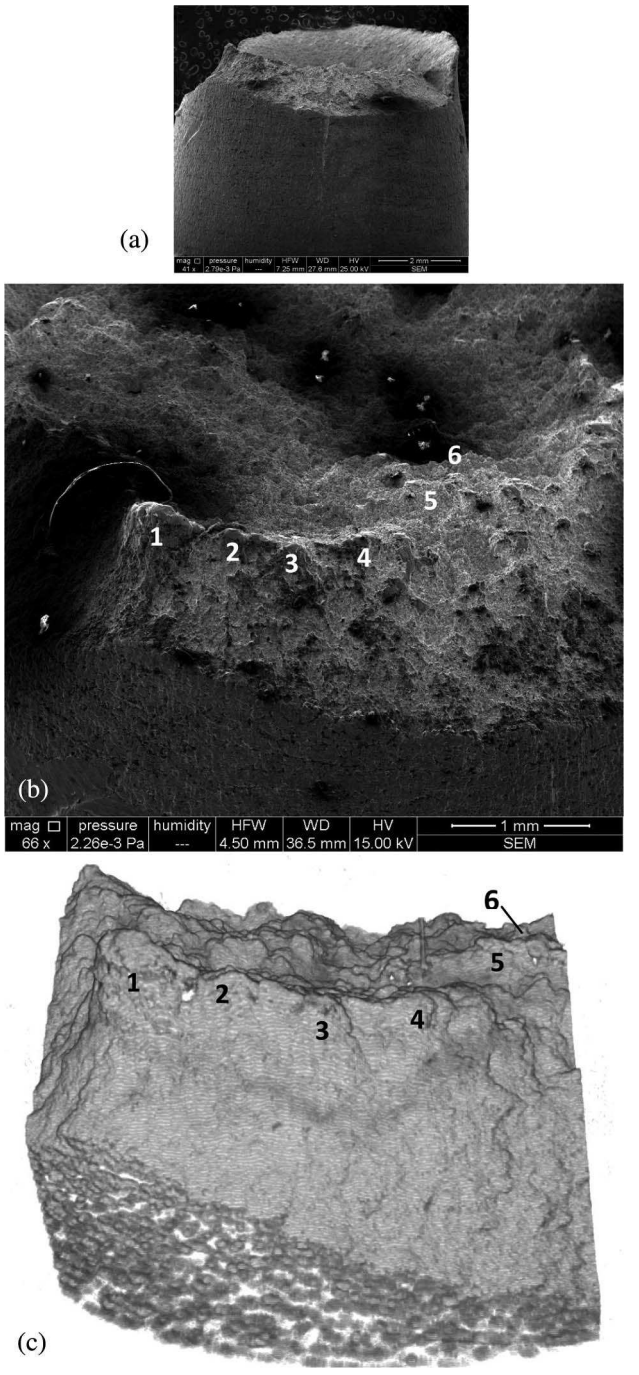

Fig. 3. Imaging the fracture of OL 52 steel: (a) SEM overview of the entire sample; (b) SEM image; (c) OCT image of the same area.

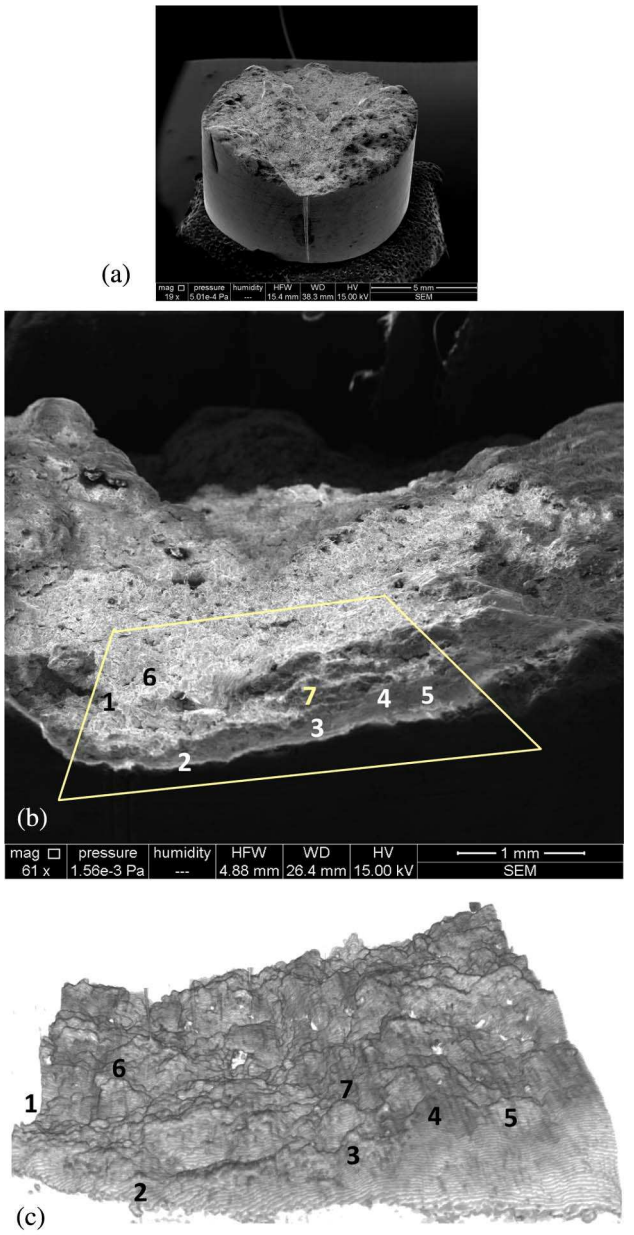

Fig. 4. Imaging the fracture of the Sn–Sb–Cu antifriction alloy: (a) SEM overview of the entire sample; (b) SEM image; (c) OCT image of the same area.

image. Figure 4(c) shows the OCT image of the microstructure on this area. A validation of the OCT image is made by using the seven grains counted and identified on both images. The same topography is thus noticed on both the OCT and SEM images.

The way some grains broke in a transgranular manner and others in an intergranular one can also be seen on both images, SEM and OCT. This is specific to the brittle fracture of metallic materials, achieved by cleavage and consisting in the breakdown of atomic bonds between atoms situated on two adjacent planes perpendicular to the direction in which the normal tensile stress/load is applied. A cleavage fracture may occur through the crystal grain (as seen on grain 6, for example) or at crystal grain boundaries (as seen on grains 2–4 and 7, for example).

4. Conclusion

Images showing surface microstructures of a steel metallic alloy and of an antifriction alloy previously subjected to ductile or brittle fracture were generated using two different imaging technologies, OCT and SEM.

The analysis of these microstructures showed that the images obtained via OCT at 10 μm overall

resolution are compatible with the SEM images at 4 nm resolution—for this specific application. Therefore, the study demonstrated that OCT can replace the costly and time-consuming SEM in the analysis of surface microstructures in the case of metallic materials that have been broken in a ductile or brittle manner. It is essential to determine if a material has been broken in a ductile or brittle manner under operating conditions. As was pointed out from the beginning, the ductile fractures do not occur instantly, as the brittle ones do. As an elongation takes place before the actual fracture, there are less serious problems in the case of ductile fractures than of brittle fractures.

Another advantage of opting for OCT instead of an SEM is the possibility of assembling small, compact OCT mobile units and handheld scanning probes [18–22]. Such units make on-site evaluations possible. This is essential in the case of aviation, maritime, road, or rail accidents, for example, but also in other types of applications, such as military ones, where on-site analysis of different fracture incidents is necessary. Also, in contrast to the SEM, for which samples have to be cut from the respective machinery part, the OCT analysis of the damaged parts can be performed noninvasively.

This report may also open avenues for the study of more complex fatigue fractures of metallic materials, which are responsible for numerous failures occurring under operating conditions. They take place when metallic materials are subjected to variable loads and high amplitudes. The resistance and ductility of the materials therefore decrease, and fracture occurs at lower tensile stress values than their tensile strength or even their flow stress. In fatigue fractures, there are three different areas at microstructure level: the crack initiation area (in a ductile manner, over several grains), the fatigue fracture area (with fiery lines), and the final fracture (brittle or ductile). Such combinations of different types of fractures are the subject of future work.

This work was supported by a Partnership grant of the Romanian Authority for Scientific Research, CNDI–UEFISCDI project code PN-II-PT-PCCA-2011-3.2-1682 (http://3om-group-optomechatronics.ro/). A. Bradu and A. Podoleanu acknowledge the support of the ERC COGATIMABIO 249889. A. Podoleanu is also supported by the NIHR Biomedical Research Centre at Moorfields Eye Hospital, the NHS Foundation Trust, and the UCL Institute of Ophthalmology.

References

1. D. Huang, E. A. Swanson, C. P. Lin, J. S. Schuman, W. G. Stinson, W. Chang, M. R. Hee, T. Flotte, K. Gregory, C. A. Puliafito, and J. G. Fujimoto, "Optical coherence tomography," Science **254**, 1178–1181 (1991).
2. A. Gh. Podoleanu and R. B. Rosen, "Combinations of techniques in imaging the retina with high resolution," Prog. Retin. Eye Res. **27**, 464–499 (2008).
3. K. A. Serrels, M. K. Renner, and D. T. Reid, "Optical coherence tomography for non-destructive investigation of silicon integrated-circuits," Microelectron. Eng. **87**, 1785–1791 (2010).
4. K. Wiesauer, M. Pircher, E. Gotzinger, C. K. Hitzenberger, R. Oster, and D. Stifter, "Investigation of glass–fibre reinforced polymers by polarisation-sensitive, ultra-high resolution optical coherence tomography: internal structures, defects and stress," Compos. Sci. Technol. **67**, 3051–3058 (2007).
5. M. R. Strakowski, J. Plucinski, M. Jedrzejewska-Szczerska, R. Hypszer, M. Maciejewski, and B. B. Kosmowski, "Polarization sensitive optical coherence tomography for technical materials investigation," Sens. Actuators A **142**, 104–110 (2008).
6. B. Heise, S. E. Schausberger, S. Häuser, B. Plank, D. Salaberger, E. Leiss-Holzinger, and D. Stifter, "Full-field optical coherence microscopy with a sub-nanosecond supercontinuum light source for material research," Opt. Fiber Technol. **18**, 403–410 (2012).
7. E. Jonathan, "Non-contact and non-destructive testing of silicon V-grooves: a non-medical application of optical coherence tomography (OCT)," Opt. Lasers Eng. **44**, 1117–1131 (2006).
8. W. Laopornpichayanuwat, J. Visessamit, and M. Tianprateep, "3-D surface roughness profile of 316-stainless steel using vertical scanning interferometry with a superluminescent diode," Measurement **45**, 2400–2406 (2012).
9. J. Goldstein, D. E. Newbury, D. C. Joy, C. E. Lyman, P. Echlin, E. Lifshin, L. Sawyer, and J. R. Michael, *Scanning Electron Microscopy and X-ray Microanalysis*, 3rd ed. (Springer, 2003).
10. L. Xia and C. F. Shih, "Ductile crack growth—III. Transition to cleavage fracture incorporating statistics," J. Mech. Phys. Solids **44**, 603–639 (1996).
11. T. Honomura, F. Yin, and K. Nagai, "Ductile-brittle transition temperature of ultrafine ferrite/cementite microstructure in low carbon steel controlled by effective grain size," ISIJ Int. **44**, 610–617 (2004).
12. G. T. Camacho and M. Ortiz, "Computation modeling of impact damage in brittle materials," Int. J. Solids Struct. **33**, 2899–2938 (1996).
13. Y. Tomota, Y. Xia, and K. Inoue, "Mechanism of low temperature brittle fracture in high nitrogen bearing austenitic steels," Acta Mater. **46**, 1577–1587 (1998).
14. X. Z. Zhang and J. F. Knott, "The statistical modeling of brittle fracture in homogenous and heterogeneous steel microstructures," Acta Mater. **48**, 2135–2146 (2000).
15. A. Gh. Podoleanu and A. Bradu, "Master–slave interferometry for parallel spectral domain interferometry sensing and versatile 3D optical coherence tomography," Opt. Express **21**, 19324–19338 (2013).
16. C. Marcauteanu, A. Bradu, C. Sinescu, F. I. Topala, M. L. Negrutiu, and A. Gh. Podoleanu, "Quantitative evaluation of dental abfraction and attrition using a swept-source optical coherence tomography system," J. Biomed. Opt. **19**, 021108 (2014).
17. V. F. Duma, K.-S. Lee, P. Meemon, and J. P. Rolland, "Experimental investigations of the scanning functions of galvanometer-based scanners with applications in OCT," Appl. Opt. **50**, 5735–5749 (2011).
18. W. Jung, J. Kim, M. Jeon, E. J. Chaney, C. N. Stewart, and S. A. Boppart, "Handheld optical coherence tomography scanner for primary care diagnostics," IEEE Trans. Biomed. Eng. **58**, 741–744 (2011).
19. R. Cernat, T. S. Tatla, J. Pang, P. J. Tadrous, A. Bradu, G. Dobre, G. Gelikonov, V. Gelikonov, and A. Gh. Podoleanu, "Dual instrument for in *vivo* and *ex vivo* OCT imaging in an ENT department," Biomed. Opt. Express **3**, 3346–3356 (2012).
20. C. D. Lu, M. F. Kraus, B. Potsaid, J. J. Liu, W. Choi, V. Jayaraman, A. E. Cable, J. Hornegger, J. S. Duker, and J. G. Fujimoto, "Handheld ultrahigh speed swept source optical coherence tomography instrument using a MEMS scanning mirror," Biomed. Opt. Express **5**, 293–311 (2014).
21. V. F. Duma, "Scanning in biomedical imaging: from classical devices to handheld heads and micro-systems," Proc. SPIE **8925**, 89250L (2014).
22. D. Demian, V. F. Duma, C. Sinescu, M. L. Negrutiu, R. Cernat, F. I. Topala, Gh. Hutiu, A. Bradu, and A. Gh. Podoleanu, "Design and testing of prototype handheld scanning probes for optical coherence tomography," J. Eng. Med., doi: 10.1177/0954411914543963 (posted online August 8, 2014).